Supporting information

S1. Selection of coccolithophore and diatom productivity proxies

In this study, we chose coccolith-based proxies as indicators of coccolithophore productivity, including the *F. produnda* percentage (Fp%), coccolith abundance (total nannofossils and/or family Noelarhabdaceae coccolith) in the sediment (NAb. or Noel. Ab.), coccolith accumulation rate (NAR or Noel. AR), and coccolith carbon isotope vital effect. These proxies show good correlations among each other (**Figure S1**). So, we suggest that records using these diverse indicators can be assembled to evaluate the global pattern of coccolithophore productivity.

The coccolith Sr/Ca ratio was suggested as a calcification rate proxy (Stoll et al., 2002b) and thereby, a potential productivity proxy. However, this proxy was excluded from our work based on following considerations. Culture studies show that the Sr/Ca in coccolith is actually a function of both calcification rate and calcification temperature(Stoll et al., 2002a). When the temperature component is significant, uncertainties quantifying the change in calcification temperature can contribute a large uncertainty in the estimated productivity-driven variation in Sr/Ca. For example, the calibrated Sr/Ca show a significant glacial-interglacial cycle since MIS 7 in the West Pacific Warm Pool, which was different from the *F. profunda*% records (Jin et al., 2018), suggesting problems deconvolving the temperature and productivity components, at least in some settings.

Alkenone-based proxies, including alkenone content and accumulation rates in the sediment, are also excluded from this study. We found that the published alkenone concentration on sediments do not show any global bloom-like pattern. Rather, most of the alkenone concentration or accumulation rate records have significant glacial-interglacial dynamics, which may alternatively reflect that the deep ocean ventilation and oxygen concentration have a dominant control on the alkenone preservation (Anderson et al., 2019), at least in the Pacific basin.

Regarding the diatom productivity, here we employed biogenic opal (accumulation rate and content), diatom accumulation rate, color reflection of sediment and element ratios in this study. The magnetic susceptibility (MS) is indicative of the presence of magnetic grains, thus is sensitive to lithological variations. This parameter shows an anti-correlation with biogenic particles, such as those rich in diatoms, which have very low MS usually 1-2 orders of magnitude lower than non-diatom layers (Xuan et al., 2016). Therebefore, the MS can be employed as a good indicator of diatom abundance in cores where opal, not carbonate, is the dominant biogenic mineral. The color reflectance on 650-750 nm band or b* parameter track the blue-yellow color component of the sediment. In the tropical ocean, the color reflectance of sediment carries the information of carbonate content. However, in the high latitude, because of the low carbonate content in sediments, this color reflectance has a linear relationship with biogenic opal and negative correlated with magnetic susceptibility (Kunz-

Pirrung et al., 2002; Sprenk et al., 2013), therebefore also indicating the pale diatom or diatom-nannofossil ooze(Kemp et al., 2010). The Ba-based element ratios are traditional productivity proxies, which can indicate the diatom productivity in upwelling regions where diatoms dominate (Calvert and Pedersen, 2007). In the equatorial Pacific site, TT013-PC72, Ba accumulation rates are positively correlated with opal accumulation rates but not carbonate accumulation rates (Murray et al., 2012). We found that the Ba/P ratio, but not Ba/Al nor Ba/Ti, is significantly correlated with opal% in this setting (**Figure S2**). Based on these comparisons, we select the Ba/P as a diatom productivity proxy for the results from TT013 cores from the Eastern Tropical Pacific, when direct opal % data are lacking (Murray et al., 2000).

S2. Coccolithophore and diatom productivity records

The coccolithophore productivity records employed in this study are from 18 different sites, 14 of which are published data and the rest are new data provided in this study (**Table S1**). There are benthic or plankton foraminifera oxygen isotope age models for most of cores except the two cores in the East Pacific, ODP 1237 and ODP 1238, the age model of which were established by biostratigraphy and magnetostratigraphy. The age models are based on original ones without any modification. All coccolithophore productivity records are plotted in **Figure S3** and **Figure S4**.

Thirty diatom productivity records were collated and analyzed in this study. Most of the data were obtained from the Pangea website (www.pangaea.de) or the supplementary information of original publications directly. The biogenic opal accumulation rates in site ODP 1343 (No.1 in the **Table S2**) was provided by authors via personal communication and the opal percentage in the core IODP U1341 and Opal accumulate rate in the core ODP 1145 were digitized manually. Age models of all diatom records have already been described in the original publication. The two sites in north Pacific (IODP U1341 and U1343) and sites ODP 704 and 1084 were dated by biostratigraphy and magnetostratigraphy. The age model of Southern Ocean site, PS58/254-1, was established by turning MS to LR04 benthic foraminifera oxygen isotope stack. Age models of all other sites are based on either benthic or planktonic foraminifera oxygen isotopes.

S3. Detecting the peaks of productivity

In this study we employ the cross-correlation method to detect the timing of coccolithophore bloom peak during the Mid-Brunhes period. We selected this method based on the classical theory that coccolithophores bloomed during the low eccentricity periods (Rickaby et al., 2007). The cross-correlation analyses were carried on coccolithophore productivities and eccentricity parameters (Berger and Loutre, 1991). If the peak of coccolithophore bloom coincided with the lowest eccentricity, the lowest correlation coefficient (R) should be detected at zero lead/lag. When the lowest R was found as positive lead, that represents the peak of coccolithophore bloom happened before the eccentricity minimum, and vice versa (**Figure S5**).

To facilitate comparisons, the sign of all proxies is adjusted to have a positive, rather than either positive or negative, correlation with productivity. For example, we used the (1-Fp%) in the following analyses instead of Fp% directly, since Fp% is negatively correlated with satellite-based primary productivity estimates in tropical and subtropical oceans(Beaufort et al., 1997; Hernández-Almeida et al., 2019; Zhang et al., 2016). All downcore results are datasets sampled unevenly. Thus, before carrying out the cross-correlation, the coccolithophorid productivity records were interpolated into 1 kyr time resolution, same as the resolution of the orbital parameters. For unevenly sampled data, there is no analytical way to estimate the significance and error of cross correlation results (Misra et al., 2018) and the usage of this method could be challenged by the sampling resolution. To test the robustness of this method on datasets with different time resolutions, we resample the Fp% result of site ODP 807, the dataset with the highest original temporal resolution, with different resolutions (from 5 kyr to 40 kyr) and use a Monte Carlo process to test how the robustness varies with sampling resolution (**Figure S6**).

The results plotted in **Figure S7** show that the cross-correlation analyzed in Monte Carlo simulations turned to more scattered after decreasing the resample resolution. When the resampling resolution decreased to 30 kyr per sample, the cross-correlation results was about 10 kyr different compared the original results (**Figure S7**). As described in the results section, the timing difference between low latitude and high latitude coccolithophore bloom is about 60-90 kyr and the lowest average sampling resolution employed in this study is ~26 kyr per sample (site IODP U1304) resulting in an error of about 30 kyr. All datasets from the Western Pacific have resolutions higher than 20 kyr per sample. Hence, we suggest that the sampling resolution in this study does not influence the main conclusions in this work.

Moreover, we also observe that the coccolithophore bloom events were not always be detected during the eccentricity minimum in sites ODP 1209, MD90-0936, IDOP U1304 and the Portugal Stack, based on the cross-correlation results. For example, the coccolith accumulation rates in the site ODP 1209 show a significant peak around 600 ka, which could be controlled by the dynamics of continental-derived dust and the Kuroshio current (Bordiga et al., 2014; Lupi et al., 2019). The cross-correlation between productivity in ODP 1209 and eccentricity shows similar negative values from -150 kyr to 5 kyr (**Figure S5**) suggesting that there is no significant bloom event in this site during the eccentricity minimum. For the site MD90-0936, the positive correlation between eccentricity and coccolithophore productivity (1-Fp% in this case) at zero lead/lag is more significant than the negative correlation at -180 kyr. This suggests that the peak of coccolithophore productivity in this site co-occurred with the eccentricity maximum instead of minimum. The situations are similar for the records from IODP U1304 and the Portugal Stack (**Figure S5**). In conclusion, we suggest that there were no significant coccolithophore bloom during the eccentricity minimum in these four sites.

For diatom productivity records, since there is no reported significant global diatom productivity trend in the Pleistocene, as there is for coccolithophore productivity records, the cross-correlation method is not suitable for detecting the phase relationship with eccentricity here. Instead, we

employ a peak searching algorithm to find out the high diatom productivity periods. Here we defined the high productivity period as a period when the productivity is higher than the threshold in a window. The window width is 200 kyr and the threshold is the mean value in the sampling window plus 2 standard deviation (std). Different selections on window length and threshold could lead to different peak timing. Here we test and discuss the influences from window length and threshold using the records of Opal% from the IODP site U1338 (highest resolution diatom productivity dataset in this study). The peak of Opal% data were calculated using window lengths varying from 100 kyr to 1000 kyr and thresholds varying from 1 to 2.7 std. The results show that the variations of threshold and window width do not significantly change the timing of peaks (**Figure S8**).

S4. Coccolith carbon isotope vital effect and size

The recent development of coccolithophore isotopic simulations and the accumulation of culture data has enabled estimations of coccolithophore growth rates from sedimentary coccolith and alkenone carbon fractionation data (McClelland et al., 2017). Unfortunately, paired coccolith and alkenone carbon isotope fractionations are not available in this study. Here we only discuss the potential trend of the growth rate from the MIS 13 to MIS 9, which is the key period for the Western Pacific coccolithophore bloom event.

In McClelland et al's (2017) model, heavier coccolith carbon isotope values represent higher growth rates/ larger cell sizes/lower atmospheric CO_2. This is caused by a more significant carbon limitation, which leads to use the bicarbonate pump by coccolithophores to transport the bicarbonate (about 9 per mil heavier in carbon isotope than CO_2) into cell (McClelland et al., 2017). The average separated coccolith sizes varied in a narrow ranged from 3.2 µm to 3.8 µm from the MIS 13 to MIS 9 and the CO_2 concentration during MIS 11, MIS 9 were similar (**Figure S10**). The sea surface temperatures during this period is not available at the site ODP 807, but according to sites nearby, the sea surface temperature did not change much during each of these interglacial periods (Dyez and Ravelo, 2014). Moreover, we did not find any significant differences in coccolith size and species after separation between the 300 ka and 400 ka samples (**Figure S11 b-c**), when the coccolith carbon fractionations in these two samples are about 1 per mil different. Considering all these facts, we suggest that the coccolith carbon isotope fractionation could be interpreted as higher growth rate in MIS 9 lead to more positive carbon isotope in coccolith, at least during the MIS 13-9 period.

S5. The nutrient pattern in modern ocean

Si/P ratios in the modern ocean were derived from the original silicate and phosphate concentration in the WOA13 dataset (Garcia et al., 2013). As illustrated in **Figure 2**, the negative correlation between Si/P ratio and bloom timing is significate, indicating that the bloom events happened firstly around the low eccentricity period at the ocean regions with high Si/P ratios today (**Figure 2a**). In other words, the coccolithophore bloom pattern during the MIS 13 is analogous to conditions that enable elevated seasonal concentrations of

coccolithophores in the so-called the 'Great Calcite Belt', near the sub-Antarctic front (Balch et al., 2011). This could be caused by lack of silicate limiting the growth of competing diatoms.

We also compared the modern Si/N ratio with the bloom timing at each site. The result also shows a significant negative correlation (**Figure S12**, R = -0.72). Further comparison between different nutrient concentrations and bloom timings show weak correlations between them (**Figure S12 b-d**) suggesting that type of dissolved nutrients play more important role in coccolithophore global bloom pattern instead of nutrient concentration. However, we believe that the phosphate may play more important roles in turning the global algae bloom rhythm and pattern, especially coccolithophores' bloom, based on the following reasons. (1) The Ca-P bodies found in coccolithophore suggests that P plays important roles in calcium transport and thereby in calcification of coccolithophore (Sviben et al., 2016). (2) The blooms of *E. huxleyi* in modern ocean happen in a high P/N ratio environment (Lessard et al., 2005) suggesting a closer relationship between phosphate and coccolithophore productivity. (3) Although algae are always directly limited by the nitrogen in modern ocean, the lack of phosphate could lead to limitation of nitrogen fixed by bacteria eventually causing the limitation of marine productivity (Paytan and Mclaughlin, 2007). (4) On geological time scales, the phosphate supply to ocean controlled by weathering and fluvial transport ultimately limits the marine productivity (Tyrrell, 1999).

S6. Length of coccolithophore growth season around the polar front

Before the disscussion in this section, we should notice that the concept of modern coccolithophore bloom is different from the 'bloom' that we have discussed in this work. The modern bloom was defined as the cyclic variation of particle inorganic carbon (PIC) or chlorophy concentriation detected by statellite, which is a seasonal event. In the sedimentary records, the coccolithphore bloom refers to the increase in cococlithophore productivity integrating thousands of 'modern-bloom' events.

The light is the main limation of alage growth in high-latitude winter besides temperature (Nissen et al., 2018). In the modern Southern Ocean, coccolithophores grow from spring to summer and the growth season could last about 3 months based on the statellite observation (Hopkins et al., 2015) and their results show that coccolithophore blooms last 162±22 days in the Southern Ocean Pacific section, which indicated that the insolation threshold of bloom could be around 350 W m^{-2}. Considering the fact that the most abundant coccolithophore species during the last low eccentricity period (about 400 ka) is the *Gephycapsa caribbeanica*, with heavier calcification than the species found in modern-bloom events, *E. huxleyi*, the bloom insolation threshold could be higher in the past than that in modern ocean. Here we test different insolation threshold ranging from 350 W m^{-2} to 450 W m^{-2} in latidutes between 40°S to 65°S and define the coccolithophore bloom length as the number of days when the daily insolation is larger than the threshold in one year. The daily insolation was calculated by a matlab function 'daily_insolation.m' (Huybers, 2006) with orbital parameters (Berger and Loutre, 1991). The results of 'bloom duration' is shown in **Figure S13**.

The estimated bloom durations show both highest and lowest values aroud 200 ka, when the eccentricity was largest, in all threshold tested in this study. That means, if the insolation was the main driver of cococlithophore bloom in the Southern Ocean, the peak of coccolithophore

productivity should be found during the precession peak in high eccentricity period. However, significant productivity can only be witnessed in the low eccentricity periods between 500 ka and 400 ka in the Southern Ocean, depending on latitude, suggests that factors other than insolation controlled coccolithophore bloom timing.

In order to test the insolation effect in coccolithophore blooms in the Southern Ocean, we estimated how long should the bloom be extended to produce a 10 times increase in productivity compared with non-bloom periods, as observed in the sites ODP 1089 and 1170. The algae cell number increase after time, t, can be described by the following euqation:

$$\frac{N_t}{N_0} = exp^{\mu \times t}$$

Where the N_t/N_0 is the how the number of cells has increased at time 't' compared with the initial cell number, and μ is the growth rate. The results of increase time in different growth rates are plotted in **Figure S14**. For example, with a growth rate of 1.2 day^{-1}, a coccolithophore community need a 1.8 times longer annual bloom duration to form a 10 times higher paleoproductivity peak compared with the 'non-bloom' periods. Considering a much lower coccolithophore growth rate in the Southern Ocean(Krumhardt et al., 2017), the bloom duration in a signle year should be extened to more than five times (500%) than the bloom duration in low coccolithophore productivity periods (aroud 200 ka). However, as shown in **Figure S13**, the variation of bloom duration is within 100% for latitudea around 50-60°S and even less in the sub Antractic zone. With these simple calculations, we suggest that the length of growth season triggered by insolation cannot expalin the coccolithophore bloom during the low eccentricity periods.

S7. Coccolithophore bloom in Eastern Pacific

There is about 20 kyr lag between the coccolithophore bloom in the Eastern Pacific upwelling zone and the coccolithophore bloom in the Sub Antarctic Front of the Southern Ocean (**Figure 2b** and **Figure 5**). Based on the silicate leakage theory, when diatoms consume the dissolved silicate in the Southern Ocean, the coccolithophore should bloom in the Eastern Equatorial Pacific upwelling zone, with a lag of at most a few thousand years. However, in this study we found the coccolithophore bloom in both the East Pacific and Benguela Upwelling zone 20-40 kyr lag to the eccentricity minimum. This kind of lag could be partly caused by the system error in cross-correlation analyses as described in the **S3**. But we suggest that the main reason for this kind of lag could be the result of a mixing between tropical climate forcing with the silicate leakage signal from high latitude (**Figure 6**). If the coccolithophore productivity is more influenced by the high-latitude process, namely the silicate leakage, the coccolithophore bloom should show smaller or no lag to the eccentricity. For the sites in the Western Pacific, where the monsoon's influence cannot be ignored, coccolithophore bloom had a longer lag than that in the Eastern Pacific region.

The modern ocean PIC concentration is a good indicator of coccolithophore productivity (Balch, 2018). Here we show that the modern East Pacific PIC concentration in the three ODP sites, ODP 1237, ODP 1238 and ODP 1240 are similar (**Figure S15**) and thereby, the coccolithophore productivity in the upper ocean among these sites should be also similar. Hence, the great difference in coccolith abundance could be mainly caused by the dissolution effect due to the different water depths of the sites.

S8. Simulating the nutrient source for coccolithophore bloom by insolation

We assumed that processes influencing coccolithophore nutrient availability are directly driven by Earth's orbital parameters, namely eccentricity and precession. (1) The nutrient leaking from latitude is controlled migration of polar front in 400 kyr^{-1} cycles. (2) The nutrient supplied by weathering is controlled by precession which is enveloped by 100 kyr^{-1} eccentricity signals.

$$N_L = A_L \times \left[\frac{1}{2}\sin\left(\frac{2\pi}{400} \times t + \theta_1\right) + \frac{1}{2}\sin\left(\frac{2\pi}{100} \times t + \theta_2\right)\right]$$

$$N_{MH} = A_{MH} \times \sin\left(\frac{2\pi}{400} \times t + \theta_3\right)$$

$$N_{cocco} = N_L + N_{MH}$$

where the N_L is coccolithophore available nutrient from low latitude process, the N_{MH} is coccolithophore available nutrient from Mid-high latitude and N_{cocco} is coccolithophore available nutrient in total. The shapes of nutrient available signals are tuned by two parameters, the amplitude of the two signal (A) and the phase of them (θ). Considering the monsoon intensity could be controlled by precession which is eventually enveloped by eccentricity, we use the eccentricity-like curve to simulate the nutrient from low latitude process. Given a θ_1 = 5/4 pi and θ_2 = 5/2pi, we can simulate that two peaks occurred at 200 ka and 300 ka (**Figure 6f**). Given the θ_3 = 1/2 pi, we can simulate the long eccentricity variation of nutrient leaking from the Southern Ocean (**Figure 6d**). The relative magnitude of two amplitudes, A_L and A_{MH}, controls which process plays a more important role in nutrient supply. When AL is larger, the coccolithophore available nutrient is mostly from low latitude processes, and when AMH is larger, the coccolithophore bloom is fueled by Mid-High latitude processes (**Figure S16**).

The concept model described here only provide a new perspective on how the nutrient source from different processes in the ocean could influence the phytoplankton bloom and thereby the carbon cycle. More sophisticated simulations are necessary for a better understanding the role of coccolithophore bloom in carbon cycles, especially on the phase relationships among different processes.

Tables and Figures in supplementary

Table S1. Data source of coccolithophore productivity in the last 0.8 Myr: The Noel. Ab, Noel. AR, Noel. MAR represent Noelaerhabdaceae family coccolith Abundance, Accumulation rate, carbonate Mass Accumulation Rate, respectively. The Fp% means *F. profunda* percentage. The $\delta^{13}C_{lith\text{-}DIC}$ is the coccolith carbon isotope vital effect. The age models with * are based on biostratigraphy.

No.	Site	Depth (m)	Lon.	Lat.	Noel./N Ab	Noel./N AR	Noel. MAR	Fp%	$\delta^{13}C_{lith\text{-}DIC}$	Age model Ref.	Data Ref.
1	**IODP U1304**	3046	-33.53	53.06	√	√				Xuan et al. (2016)	**This study**
2	**MD01-2446**	3570	-12.62	39.06		√				Marino et al. (2014)	Marino et al. (2014)
3	**ODP 975**	2415	4.51	38.89	√					Lourens (2004)	Maiorano et al. (2016)
4	**IODP U1385**	2578	-10.12	37.57		√				Hodell et al. (2015)	Maiorano et al. (2015)
5	**ODP 977**	1984	-1.96	36.03		√					
6	**IODP 1209**	2387	158.50	32.65		√				Bordiga et al. (2013)	Bordiga et al. (2014); Lupi et al. (2019)
7	**MD06-3050**	2967	124.78	15.95				√		Sun et al. (2011)	Sun et al. (2017)
8	**MD05-2901**	1454	110.74	14.38				√		Li (2007)	Su et al. (2013)
9	**ODP 1143**	2772	113.28	9.37	√	√	√			Tian et al. (2002)	**This study**
10	**MD90-0963**	2446	73.54	5.04				√		Bassinot et al. (1994)	Beaufort et al. (1997)
11	**ODP 807**	2804	156.62	3.61	√	√		√	√	Jin et al. (2011)	**This study**
12	**IODP 1240**	2921	-86.45	0.02		√				López-Otálvaro et al. (2008)	López-Otálvaro et al. (2008)
13	**KX21-2**	1897	157.89	-1.25				√		Zhou et al. (2011)	Liang and Liu (2018)
14	**ODP1238**	2203	-82.78	-1.87		√				Álvarez et al. (2010)*	Álvarez et al. (2010)
15	**ODP1237**	3212	-76.38	-16.00		√				Álvarez et al. (2010)*	Álvarez et al. (2010)
16	**ODP 1082**	1280	11.82	-21.09		√				Jahn et al. (2003)	Baumann and Freitag (2004)
17	**ODP 1089**	4620	9.89	-40.94	√					Hodell et al. (2001)	Flores et al. (2003)
18	**ODP 1170**	2704	146.05	-47.15	√	√				Li et al. (2010)	**This study**

Table S2. Data source of diatom productivity: BiOpal AR is biogenic opal accumulation rate, Biopal% is biogenic opal content. MS is magnetic susceptibility.

No.	Site	Lon.	Lat.	Depth (m)	Proxy	Ref.
1	IODP U1343	-175.82	57.56	1950	BioOpal AR	Kim et al. (2014)
2	IODP U1341	179.01	54.03	2139	BioOpal%	Kanematsu et al. (2013)
3	MD01-2414	149.58	53.20	1123	BioOpal%	Lattaud et al. (2019)
4	IODP U1304	-33.53	53.00	3064	MS	Xuan et al. (2016)
5	ODP 882	167.60	50.36	3243	BioOpal AR	Haug et al. (1999)
6	SO202	164.44	38.01	5102	BioOpal%	Korff et al. (2016)
7	ODP 798	134.80	37.04	914	BioOpal%	Dunbar et al. (1992)
8	ODP 1145	117.63	19.58	3175	BioOpal AR	Wang et al. (2007)
9	TT013-114	-139.85	4.04	4432	Ba/P	Murray et al. (2000)
10	IODP U1338	-117.94	3.00	4200	BioOpal%	Lyle and Baldauf (2015)
11	TT013-83	-140.15	2.07	4414	Ba/P	Murray et al. (2000)
12	TT013-72	-139.40	0.11	4298	BioOpal AR	Murray et al. (2012)
13	TT013-72	-139.40	0.11	4298	Ba/P	Murray et al. (2000)
14	ODP 664	-23.23	0.11	3806	BioOpal%	Ruddiman and Kutzbach (1989)
15	ODP 663	-11.88	-1.20	3706	BioOpal%	Ruddiman and Kutzbach (1989)
16	TT013-18	-139.71	-1.84	4354	Ba/P	Murray et al. (2000)
17	TT013-32	-139.74	-4.96	4236	Ba/P	Murray et al. (2000)
18	ODP 1084	13.03	-25.51	1991	BioOpal%	Lange et al. (1999)
19	SUSAS_stack	-16.00	-29.00	--	MS	Schmieder et al. (2000)
20	MD02-2588	25.50	-41.20	2907	BioOpal%	Romero et al. (2015)
21	MD02-2588	25.50	-41.20	2907	Diatom Ab	Romero et al. (2015)
22	ODP 1123	-171.50	-41.78	3290	Ba/Al	Hall et al. (2001)
23	ODP 1090	8.90	-42.91	3698	BioOpal%	Diekmann and Kuhn (2002)
24	ODP 704	7.42	-46.88	2543	BioOpal%	Fenner (1991)
25	ODP 1091	5.92	-47.09	4360	BioOpal AR	Cortese et al. (2004)
26	ODP 1091	5.92	-47.09	4360	Color 650-750	Kemp et al. (2010)
27	ODP 1093	5.87	-49.98	3626	Color 650-750	Kemp et al. (2010)
28	ODP 1094	5.13	-53.18	2807	Color 650-750	Kemp et al. (2010)
29	PS58/254-1	-108.45	-69.31	4014	Diatom Ab	Konfirst et al. (2012)
30	PS58/254-1	-108.45	-69.31	4014	BioOpal AR	Hillenbrand et al. (2009)

Table S3. Results of cross-correlation between coccolithophore productivity and eccentricity. X represents that no significant correlation was detected between coccolithophore productivity and eccentricity. If multiproxy were employed in one site, the lead/lag is the mean value of the results from different proxies. The numbers in bracket are sample resolution.

Site	Lead or lag of productivity to Ecc. Min. (kyr)							Comments
	Mean	Std.	1-Fp%	Noel. Ab	Noel. Acc	Noel. MC	Noel. MAR	
MD01-2446 / **IODP U1385**	X			-137 (1.34)				North Atlantic Stack
ODP 975 / **ODP 977**	-55.00				-55 (1.0)			Mediterranean stack
IODP 1209	X				-105 (7.57)			No significant peak
ODP 1240 / **ODP 1237** / **ODP 1238**	-28			-28 (6.83)				East Pacific stack
ODP 1082	-50.00			-50 (5.6)				
ODP 1089	-11.00				-11 (3.5)			
IODP U1304	X			-134 (26.6)	200 (26.6)			
ODP 1170	-3.00	3.00		-6 (15.8)	0 (15.8)			
ODP 807	-70.66	5.56	-63(3.1)	-76 (19.4)	-73 (19.4)			
ODP 1143	-92.75	2.59		-89 (16.37)	-94 (16.37)	-92 (16.37)	-96 (16.37)	
KX21-2	-68.00		-68(1.2)					
MD06-3050	-85.00		-85(3.5)					
MD05-2901	-81.00		-81(1.0)					
West Pacific Stack	-81.00		-81(0.5)					Stacked by Fp% records
MD90-0963	X		-152 (5.57)					

Table S4. The nutrient content in the modern ocean at each site where coccolithophore bloom observed during the eccentricity minimum: the nutrient data are from WOA13 at the depth of 100m.

Nutrient / Site	[Si] (μM)	[N] (μM)	[P] (μM)	Si/P	Si/N
MD01-2446	1.93	1.20	0.32	6.09	1.61
IODP U1385	2.31	4.50	0.28	8.25	0.51
ODP 975	2.42	2.30	0.16	15.15	1.06
ODP 977	3.48	3.30	0.20	17.40	1.06
IODP 1209	6.63	3.47	0.27	24.55	1.91
ODP 1240	16.02	21.72	1.66	9.68	0.74
ODP 1237	20.84	15.28	2.35	8.89	1.36
ODP 1238	16.08	22.92	1.71	9.39	0.70
ODP 1082	10.22	21.47	1.67	6.14	0.48
ODP 1089	3.29	9.68	0.92	3.58	0.34
IODP U1304	7.76	13.01	0.91	8.56	0.60
ODP 1170	3.00	10.13	0.94	3.19	0.30
ODP 807	3.74	3.91	0.39	9.58	0.96
ODP 1143	16.05	8.77	0.80	20.06	1.83
KX21-2	2.75	4.32	0.47	5.85	0.64
MD06-3050	6.28	1.27	0.18	34.24	4.94
MD05-2901	20.05	11.61	0.91	22.03	1.73
MD90-0963	16.41	20.83	1.21	13.62	0.79

Figure S1. Comparisons among coccolith-based proxies: Noel. Abundance (Noel. Ab), Noel. Accumulation rate (Noel. AR), Noel. Mass accumulation rate (Noel. MAR), *Florisphaera profunda* percentage Fp% and *Gephyrocapsa caribbeanica* percentage (Gcarb%) from the core ODP 807, KX21-2, ODP 1143 and IODP U1304.

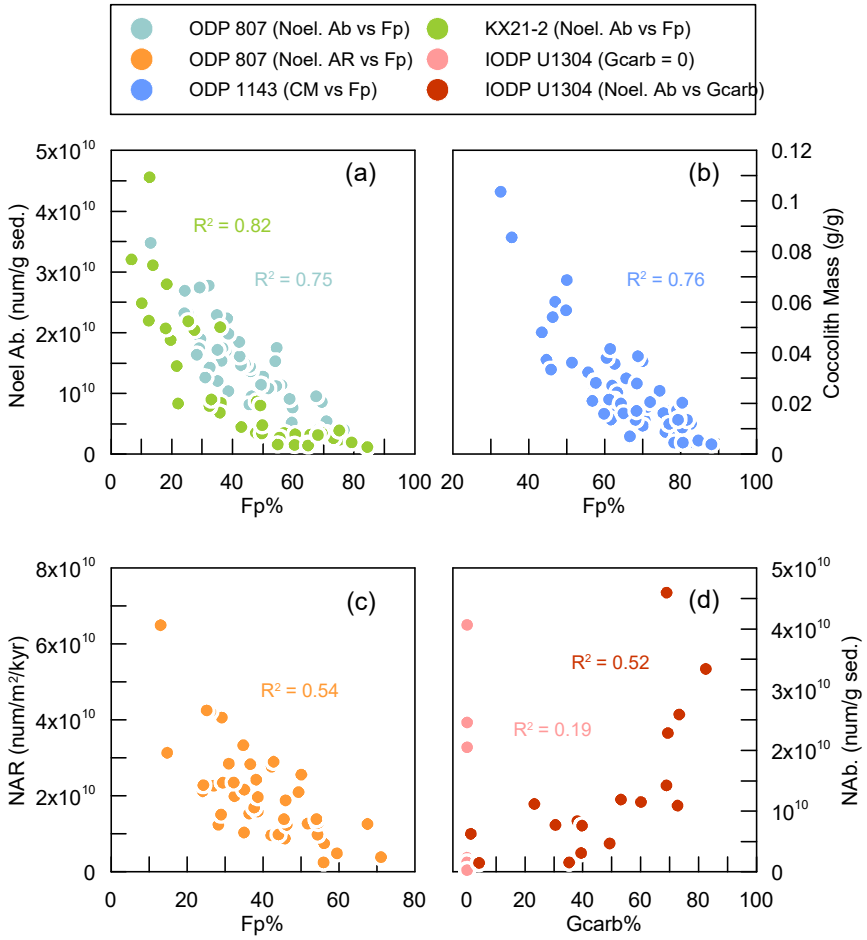

Figure S2. Si/Al, Si/P, Si/Ti and biogenic opal percentage in site TT013-PC72: Ba/P, Ba/Al, Ba/Ti (Murray et al., 2000) and Opal% (Murray et al., 2012) are paired data, thereby no data interpolations were performed before cross plotting.

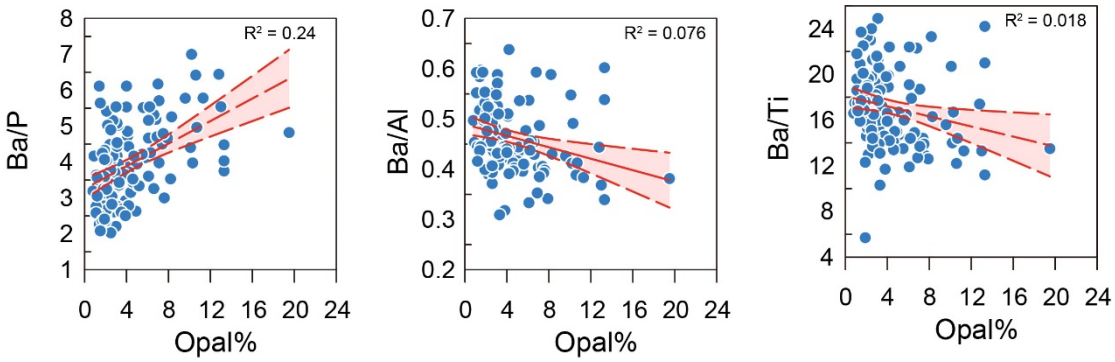

Figure S3. **Coccolithophore productivity based on Noel. AR and Noel. Ab.** The unit of Noel. AR is num. cm^{-2} kyr^{-1} and the unit of Noel. Ab. is num. g^{-1}. References for each dataset can be found in **Table S1**.

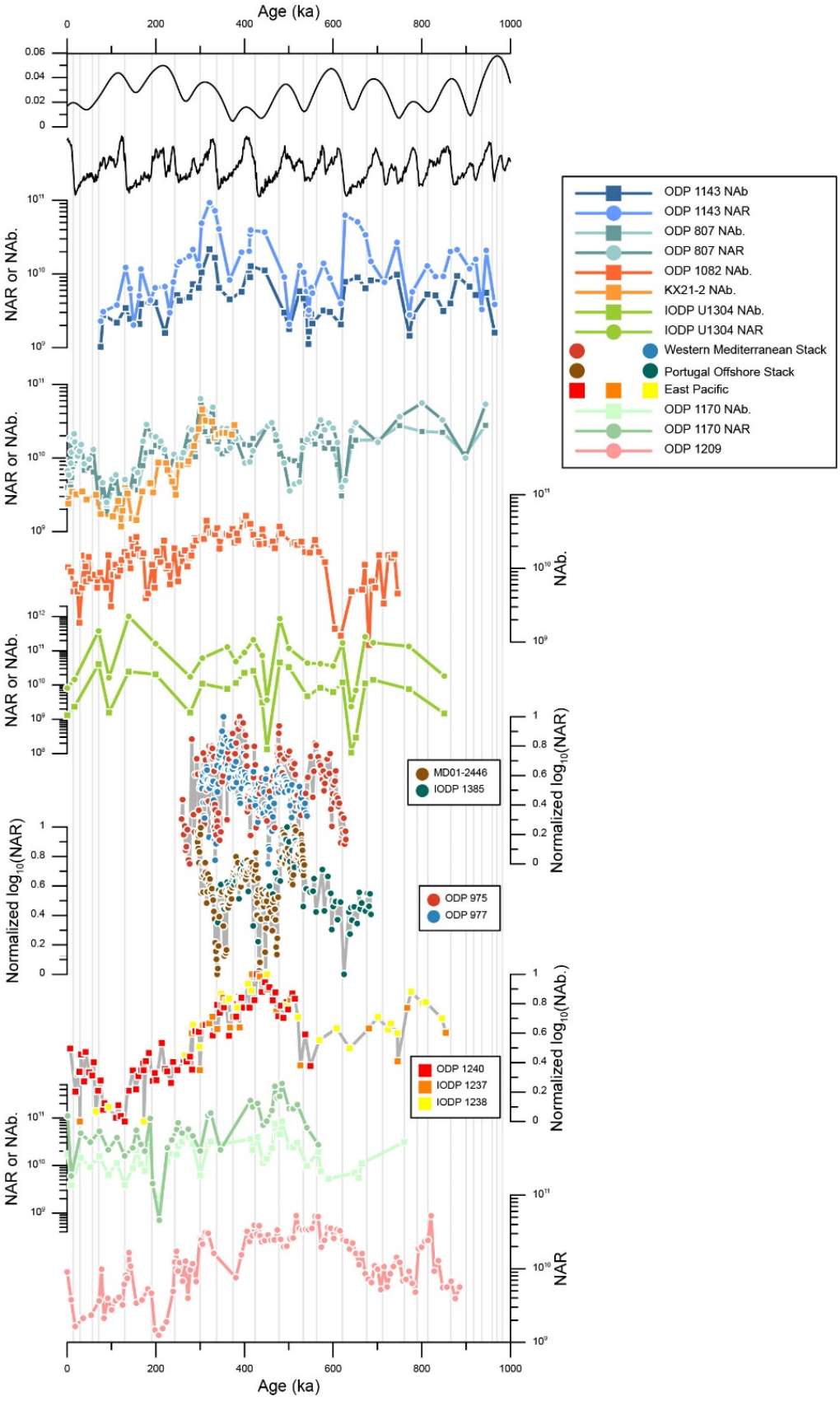

Figure S4. Coccolithophore productivity based on Fp%. References for each dataset can be found in **Table S1**.

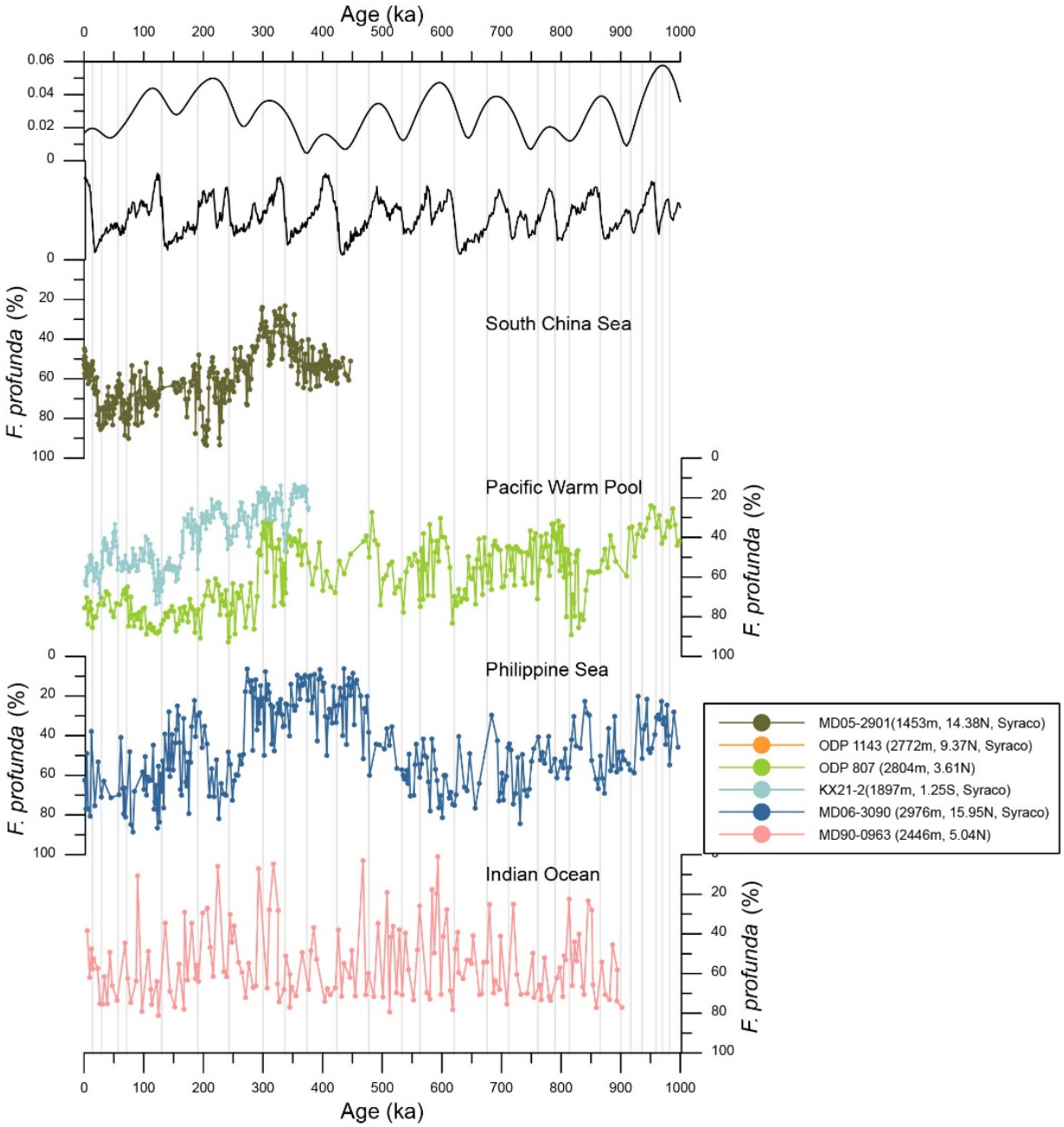

Figure S5. **Cross-correlation of different coccolith productivity records against eccentricity in the past 600 kyr:** the colors of line are same as that in the legend of **Figure 2**, with purple for Fp%, blue for NAb/Noel. Ab, green for NAR/Noel. AR, orange for Noel. MC and gray for Noel. MAR. The horizontal dashed lines represent the upper and lower confidence boundaries (±2std). Results plotted by dashed lines indicate that no significant peaks were detected during the minimum eccentricity period between 530ka and 430 ka (±100 kyr lead/lag) in this coccolithophore productivity.

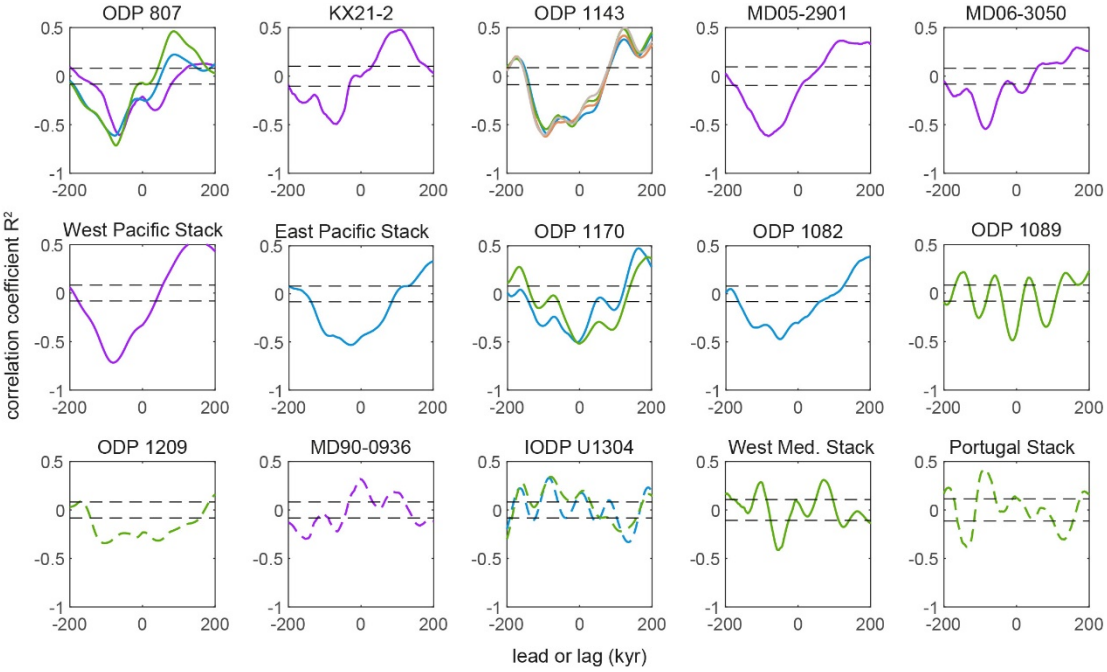

Figure S6. Error of cross-correlation analyses in the *F. profunda*% data from core ODP 807: raw data were resampled in different resolution from 5 kyr per sample to 40 kyr per sample for 1000 times, respectively. The result of cross-correlation analyses between resampled coccolithophore productivity data (time resolution of 5, 10, 15, 20, 25 kyr) and the eccentricity parameter are shown in (a-e). The lead and lag at the lowest correlation coefficient was selected as the blooming timing of coccolithophore as described in the Methods section. The difference between raw *F. profunda*% bloom timing and average resampled data timing was plotted against sampling resolution as blue line in panel (f). The orange dots and curves represent standard deviations of 1000 times repeating sampling.

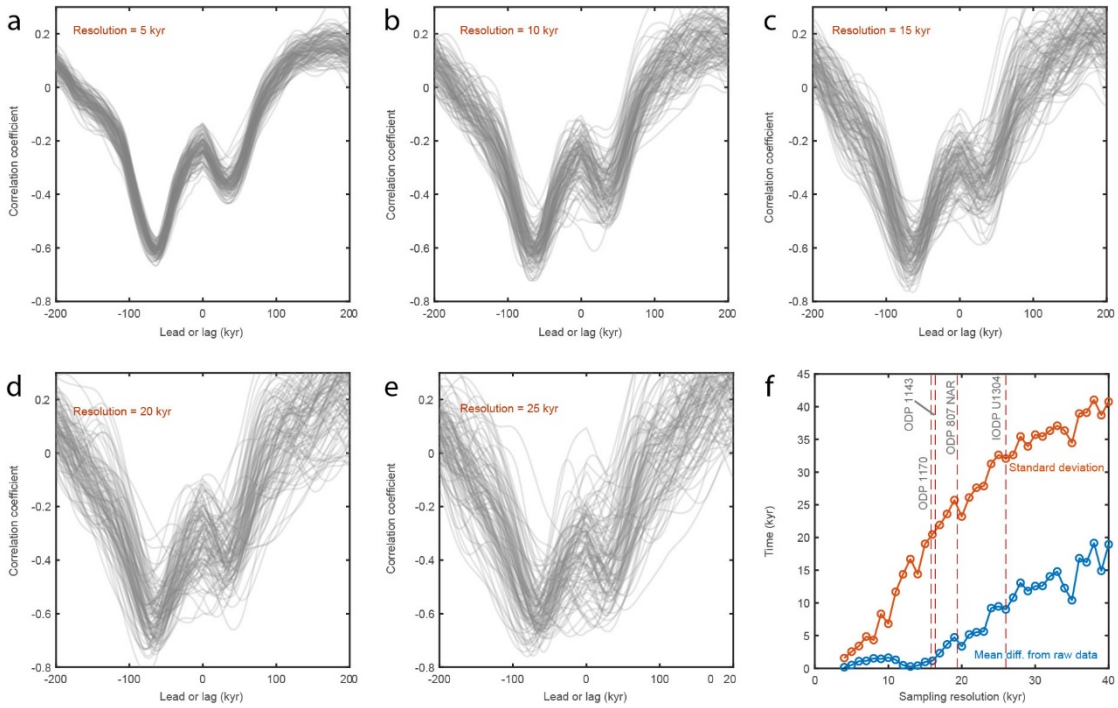

Figure S7. Detecting the peak of diatom productivity: to test the robustness of peak detecting algorithm, the biogenic opal content from core IODP U1338 was selected. The red dots in upper panel represent diatom productivity peaks detected with a threshold of 'mean value + 2 standard deviation' and 200 kyr window length. The middle panel shows that when the threshold increases, peaks will become thinner. The lower panel shows that when the window length increases, the peaks will become boarder.

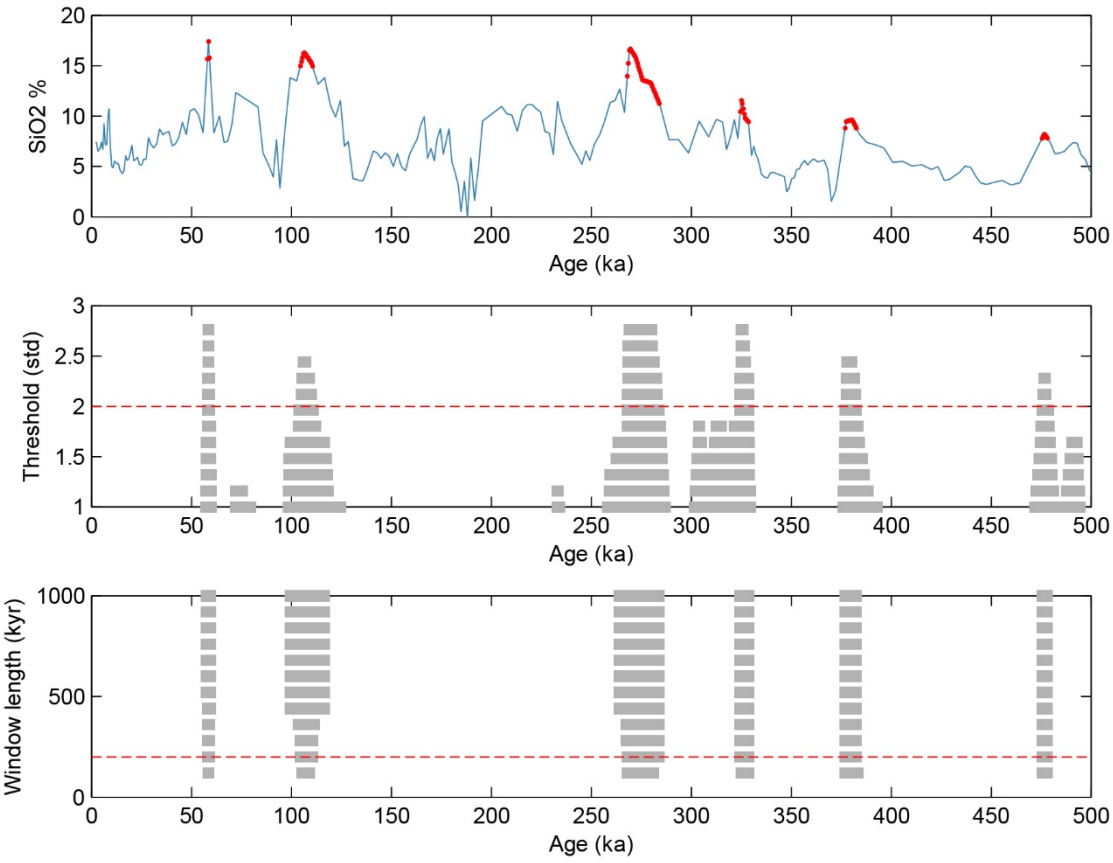

Figure S8. Diatom productivity and detected productivity peaks in the last 1 Myr: All records plotted in the left column were retrieved from the Pacific and the records in right column were from the Atlantic. The numbers on the left-up represent the latitude of sites. The red parts of the curves are where productivity peaks are detected and plotted in **Figure 4**.

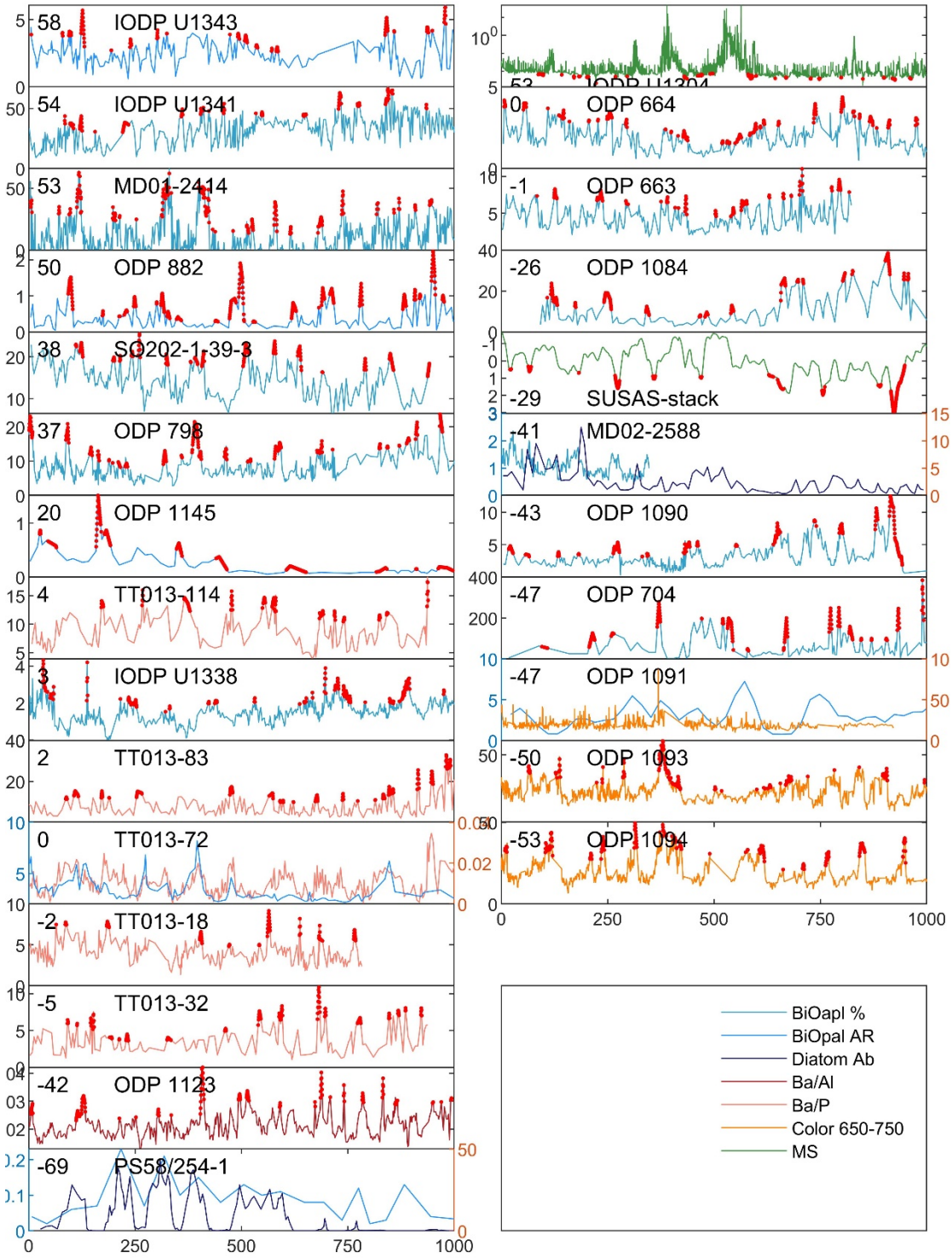

Figure S9. Seawater DIC carbon isotopes and temperature section in the modern West Pacific Warm Pool. (a) Carbon isotope in modern Pacific Warm Pool (Suzuki, 2013). (b) Temperature variation with depth and the typical living depth of *E. huxleyi* and *G. ruber*. (c) the modern data sites and location of ODP 807. If we assume the living depth between coccolithophore and *G. ruber* is about 100 meters, this would cause about 0.6 ‰ difference in the modern Pacific Warm Pool.

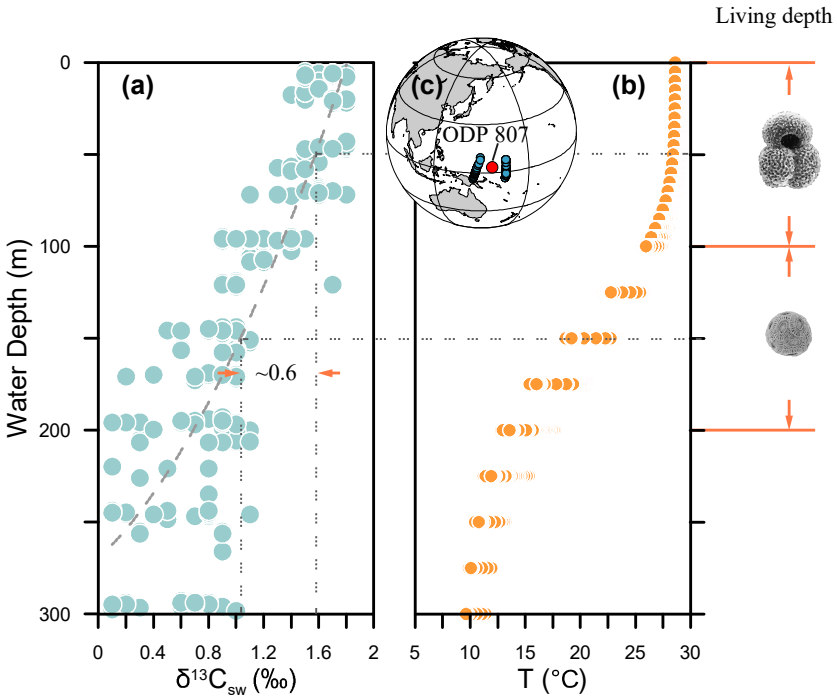

Figure S10. **Size of separated coccoliths analyzed for carbon isotopes from site ODP 807 in the Western Pacific Warm Pool**. DSL represents the Distal shade length (more detailed terminology description can be found in http://ina.tmsoc.org/terminology/3coccoliths.htm). **(a)** Coccolith carbon isotope fractionation; **(b)** atmospheric CO_2 recorded in the Antarctic ice core; **(c)** All original measurements. **(d)** Size distribution and mean length of coccolith analyzed for carbon isotope (red crosses). Red vertical bars denote the two samples which witness significant carbon isotope difference.

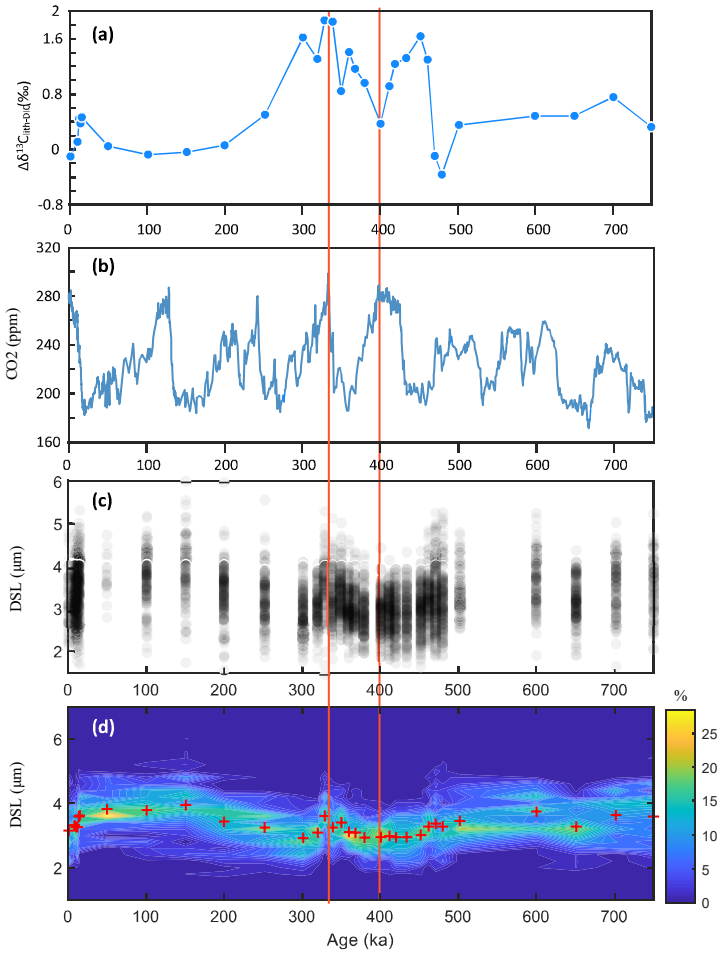

Figure S11. Potential effect from coccolith separation on carbon isotope. The four samples in (a-d) are shown in red dots in panel e and f. The coccolith number in (a) and (d) are smaller than that in (b) and (c). This is caused by two reasons: (1) the coccolith abundance in these two sample are lower; (2) and more separation times were performed in these two samples to achieve better separated coccolith fractions.

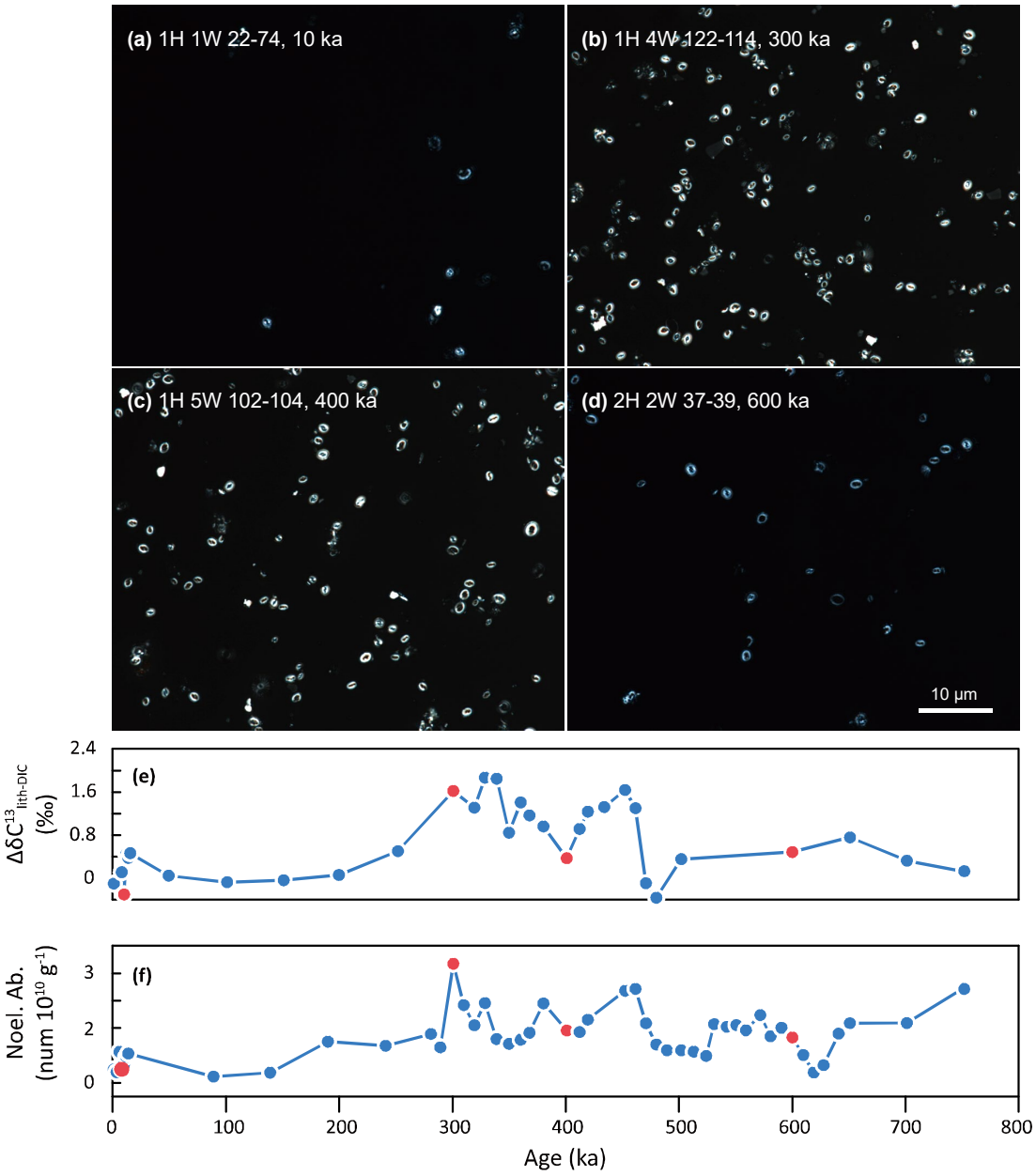

Figure S12. Bloom timing and nutrients in the modern ocean. (a) significant negative correlation between Si/N ratio and bloom timing (r^2 = 0.52); **(b)** Silicate concentration and bloom timing; **(c)** Nitrate concentration and bloom timing; (d) Phosphate concentration and bloom timing. All nutrients data are from 100 meter depth in the modern ocean (WOA13, 1°×1° annual average dataset)

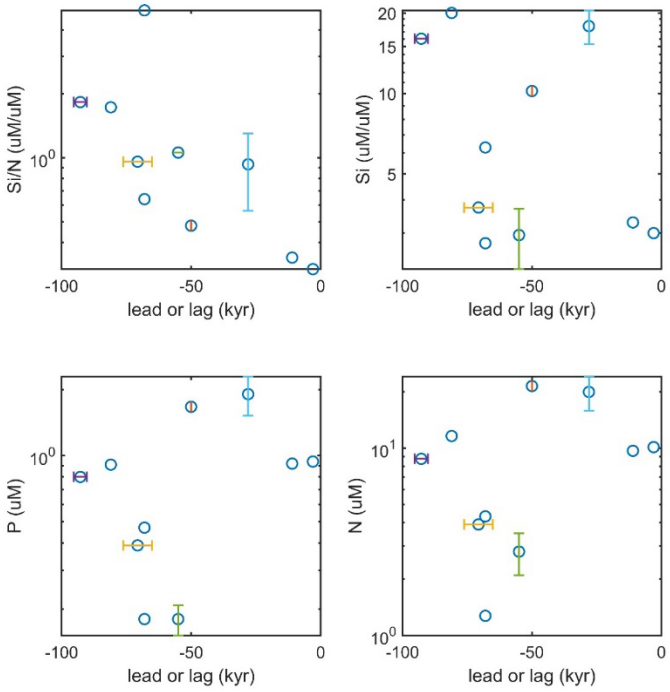

Figure S13. Algae growth season length in the last 1 Myr at the Southern hemisphere mid/high latitudes: Lines with yellow, green, black, purple and blue represent growth season calculated by thresholds of 350 W m^{-2}, 375 W m^{-2}, 400 W m^{-2}, 425 W m^{-2} and 450 W m^{-2}, respectively.

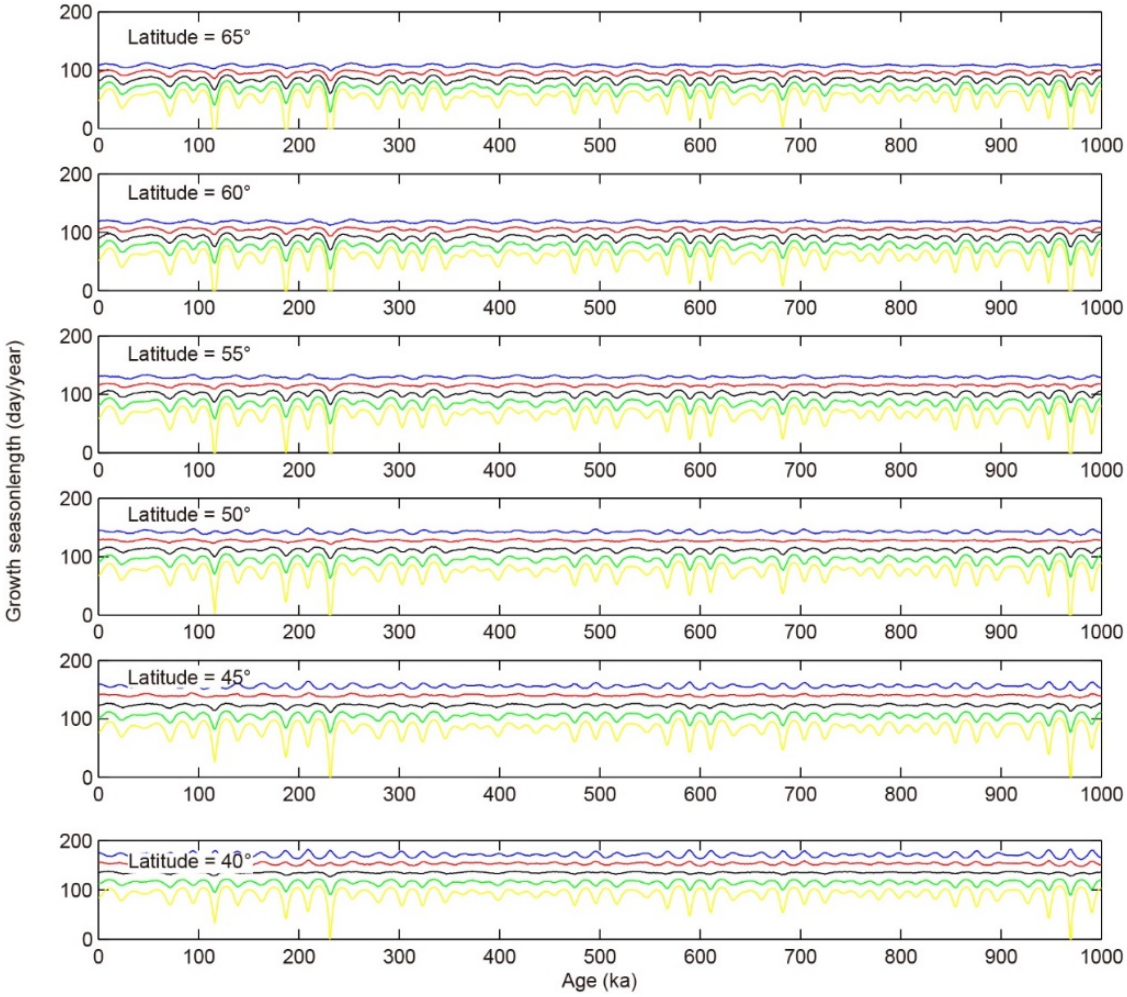

Figure S14. Cell numbers variations with time at different growth rates: the x-axis is the growth during with a unit of how long the cells have been growing (N_0). The y-axis is how many times of the cell numbers has increased. The dashed line represents the cell numbers increase one order of magnitude after a period of growing. Even in with a high growth rate of 1.2 per day, the cells still need to increase the growth duration about 1.8 times to achieve a ten-times increase in cell number.

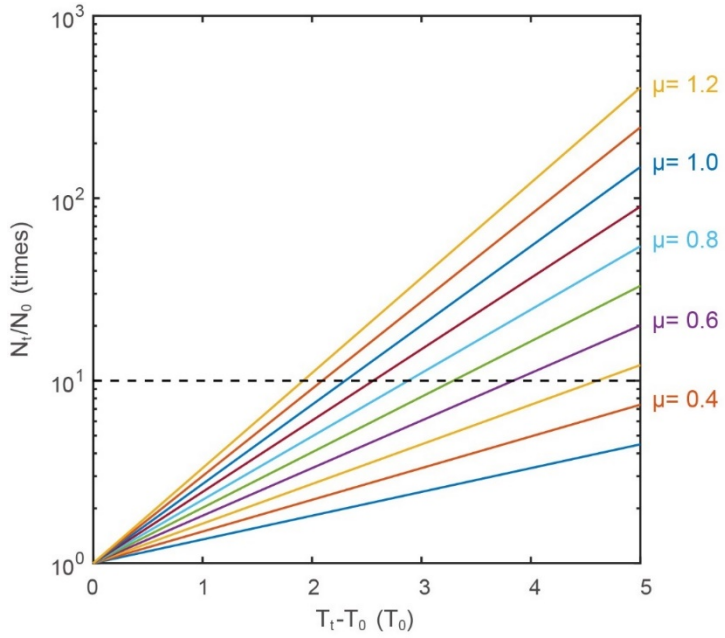

Figure S15. Coccolithophore productivity in the Eastern Pacific. The annual (a) and monthly (b) surface ocean PIC concentration data are from the 'Oceancolor' website.

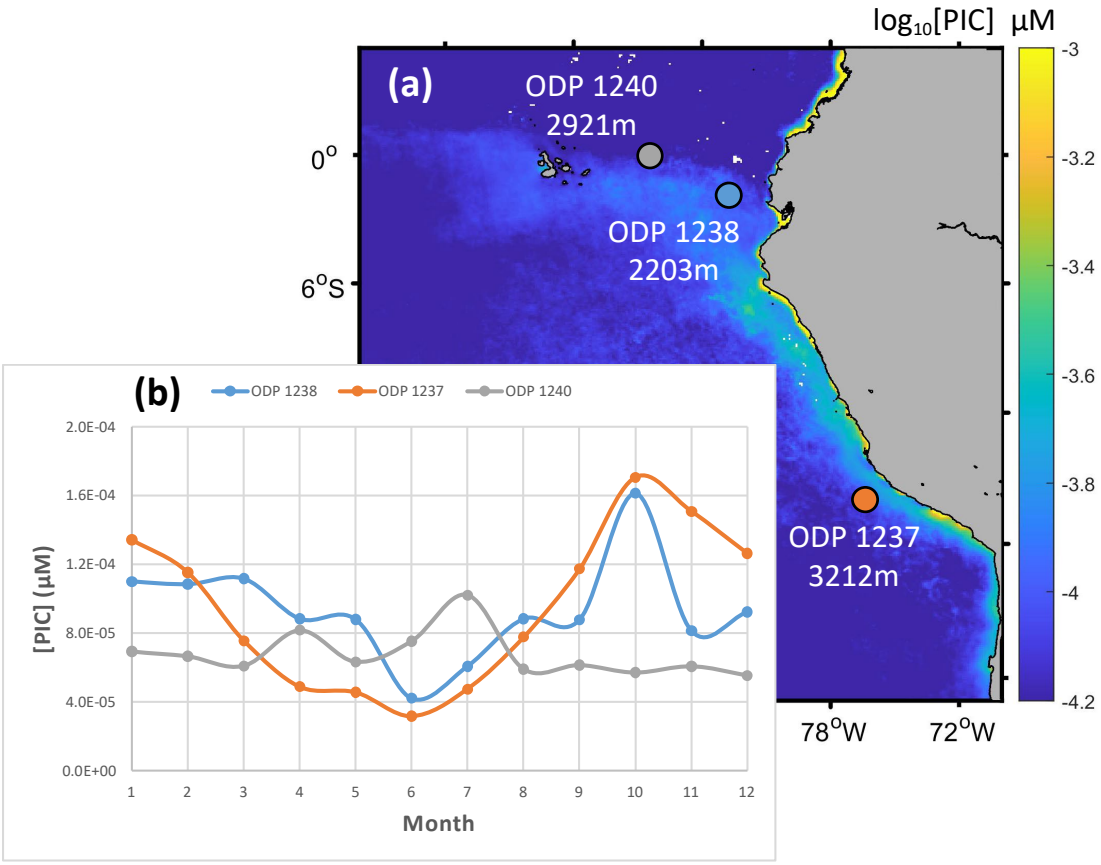

Figure S16. Simulation the diachronous coccolithophore bloom. The timing of 'bloom peak' calculated in **S8** can be tuned by the relative intensity of low and mid-high latitude process (A_L/A_{MH}). When the A_L/A_{MH} is as small as 0.1, the bloom peak appeared around 400 ka. The timing of bloom peak will shift towards 300 ka when low latitude process plays more important roles in nutrient supply.

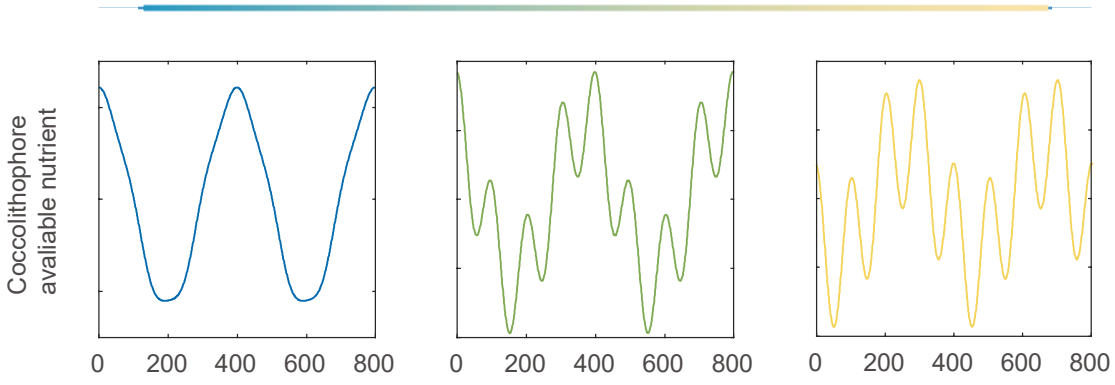

References

Álvarez, M.C., Flores, J.A., Sierro, F.J., Molina-Cruz, A., 2010. Long-term upwelling evolution in tropical and equatorial Pacific during the last 800 kyr as revealed by coccolithophore assemblages. Geobios 43, 123-130.

Anderson, R.F., Sachs, J.P., Fleisher, M.Q., Allen, K.A., Yu, J., Koutavas, A., Jaccard, S.L., 2019. Deep-Sea Oxygen Depletion and Ocean Carbon Sequestration During the Last Ice Age. Global Biogeochemical Cycles 33, 301-317.

Balch, W.M., 2018. The Ecology, Biogeochemistry, and Optical Properties of Coccolithophores. Ann Rev Mar Sci 10, 71-98.

Balch, W.M., Drapeau, D.T., Bowler, B.C., Lyczskowski, E., Booth, E.S., Alley, D., 2011. The contribution of coccolithophores to the optical and inorganic carbon budgets during the Southern Ocean Gas Exchange Experiment: New evidence in support of the "Great Calcite Belt" hypothesis. Journal of Geophysical Research 116.

Bassinot, F.C., Labeyrie, L.D., Vincent, E., Quidelleur, X., Shackleton, N.J., Lancelot, Y., 1994. The astronomical theory of climate and the age of the Brunhes-Matuyama magnetic reversal. Earth and Planetary Science Letters 126, 91-108.

Baumann, K.-H., Freitag, T., 2004. Pleistocene fluctuations in the northern Benguela Current system as revealed by coccolith assemblages. Marine Micropaleontology 52, 195-215.

Beaufort, L., Lancelot, Y., Camberlin, P., Cayre, O., Vincent, E., Bassinot, F., Labeyrie, L., 1997. Insolation cycles as a major control of equatorial Indian Ocean primary production. Science 278, 1451-1454.

Berger, A., Loutre, M.-F., 1991. Insolation values for the climate of the last 10 million years. Quaternary Science Reviews 10, 297-317.

Bordiga, M., Beaufort, L., Cobianchi, M., Lupi, C., Mancin, N., Luciani, V., Pelosi, N., Sprovieri, M., 2013. Calcareous plankton and geochemistry from the ODP site 1209B in the NW Pacific Ocean (Shatsky Rise): new data to interpret calcite dissolution and paleoproductivity changes of the last 450ka. Palaeogeography, Palaeoclimatology, Palaeoecology 371, 93-108.

Bordiga, M., Cobianchi, M., Lupi, C., Pelosi, N., Venti, N.L., Ziveri, P., 2014. Coccolithophore carbonate during the last 450 ka in the NW Pacific Ocean (ODP site 1209B, Shatsky Rise). Journal of Quaternary Science 29, 57-69.

Calvert, S., Pedersen, T., 2007. Chapter fourteen elemental proxies for palaeoclimatic and palaeoceanographic variability in marine sediments: interpretation and application. Developments in Marine Geology 1, 567-644.

Cortese, G., Gersonde, R., Hillenbrand, C.-D., Kuhn, G., 2004. Opal sedimentation shifts in the World Ocean over the last 15 Myr. Earth and Planetary Science Letters 224, 509-527.

Diekmann, B., Kuhn, G., 2002. Sedimentary record of the mid-Pleistocene climate transition in the southeastern South Atlantic (ODP Site 1090). Palaeogeography, Palaeoclimatology, Palaeoecology 182, 241-258.

Dunbar, R., DeMenocal, P., Burckle, L., 1992. Late Pliocene-Quaternary biosiliceous sedimentation at Site 798, Japan Sea, Proceedings of the Ocean Drilling Program, Scientific Results, pp. 439-456.

Dyez, K.A., Ravelo, A.C., 2014. Dynamical changes in the tropical Pacific warm pool and zonal SST gradient during the Pleistocene. Geophysical Research Letters 41, 7626-7633.

Fenner, J.M., 1991. Late Pliocene-Quaternary quantitative diatom stratigraphy in the Atlantic sector of the Southern Ocean, Ciesielski, PF, Kristoffersen, Y., et al., Proc. ODP, Sci. Results, pp. 97-121.

Flores, J.-A., Marino, M., Sierro, F.J., Hodell, D.A., Charles, C.D., 2003. Calcareous plankton dissolution pattern and coccolithophore assemblages during the last 600 kyr at ODP Site 1089

(Cape Basin, South Atlantic): paleoceanographic implications. Palaeogeography, Palaeoclimatology, Palaeoecology 196, 409-426.
Garcia, H.E., Locarnini, R.A., Boyer, T.P., Antonov, J.I., Baranova, O.K., Zweng, M.M., Reagan, J.R., Johnson, D.R., Mishonov, A.V., Levitus, S., 2013. World ocean atlas 2013. Volume 4, Dissolved inorganic nutrients (phosphate, nitrate, silicate).
Hall, I.R., McCave, I.N., Shackleton, N.J., Weedon, G.P., Harris, S.E., 2001. Intensified deep Pacific inflow and ventilation in Pleistocene glacial times. Nature 412, 809-812.
Haug, G.H., Sigman, D.M., Tiedemann, R., Pedersen, T.F., Sarnthein, M., 1999. Onset of permanent stratification in the subarctic Pacific Ocean. Nature 401, 779.
Hernández-Almeida, I., Ausín, B., Saavedra-Pellitero, M., Baumann, K.H., Stoll, H.M., 2019. Quantitative reconstruction of primary productivity in low latitudes during the last glacial maximum and the mid-to-late Holocene from a global Florisphaera profunda calibration dataset. Quaternary Science Reviews 205, 166-181.
Hillenbrand, C.D., Kuhn, G., Frederichs, T., 2009. Record of a Mid-Pleistocene depositional anomaly in West Antarctic continental margin sediments: an indicator for ice-sheet collapse? Quaternary Science Reviews 28, 1147-1159.
Hodell, D., Lourens, L., Crowhurst, S., Konijnendijk, T., Tjallingii, R., Jiménez-Espejo, F., Skinner, L., Tzedakis, P., Members, T.S.S.P., Abrantes, F., 2015. A reference time scale for Site U1385 (Shackleton Site) on the SW Iberian Margin. Global and Planetary Change 133, 49-64.
Hodell, D.A., Brenner, M., Curtis, J.H., Guilderson, T., 2001. Solar forcing of drought frequency in the Maya lowlands. Science 292, 1367-1370.
Hopkins, J., Henson, S.A., Painter, S.C., Tyrrell, T., Poulton, A.J., 2015. Phenological characteristics of global coccolithophore blooms. Global Biogeochemical Cycles 29, 239-253.
Huybers, P., 2006. Pleistocene glacial variability and the integrated insolation forcing. Science 313, 508-511.
Jahn, B., Donner, B., Müller, P.J., Röhl, U., Schneider, R.R., Wefer, G., 2003. Pleistocene variations in dust input and marine productivity in the northern Benguela Current: evidence of evolution of global glacial–interglacial cycles. Palaeogeography, Palaeoclimatology, Palaeoecology 193, 515-533.
Jin, H., Jian, Z., Cheng, X., Guo, J., 2011. Early Pleistocene formation of the asymmetric east-west pattern of upper water structure in the equatorial Pacific Ocean. Chinese Science Bulletin 56, 2251-2257.
Jin, X., Liu, C., Zhang, H., Zhou, C., Jiang, X., Wu, Z., Xu, J., 2018. Evolutionary driven of Gephyrocapsa coccolith isotopic vital effects over the past 400 ka. Earth and Planetary Science Letters 503, 236-247.
Kanematsu, Y., Takahashi, K., Kim, S., Asahi, H., Khim, B.-K., 2013. Changes in biogenic opal productivity with Milankovitch cycles during the last 1.3 Ma at IODP Expedition 323 Sites U1341, U1343, and U1345 in the Bering Sea. Quaternary international 310, 213-220.
Kemp, A.E.S., Grigorov, I., Pearce, R.B., Naveira Garabato, A.C., 2010. Migration of the Antarctic Polar Front through the mid-Pleistocene transition: evidence and climatic implications. Quaternary Science Reviews 29, 1993-2009.
Kim, S., Takahashi, K., Khim, B.-K., Kanematsu, Y., Asahi, H., Ravelo, A.C., 2014. Biogenic opal production changes during the Mid-Pleistocene Transition in the Bering Sea (IODP Expedition 323 Site U1343). Quaternary Research 81, 151-157.
Konfirst, M.A., Scherer, R.P., Hillenbrand, C.-D., Kuhn, G., 2012. A marine diatom record from the Amundsen Sea — Insights into oceanographic and climatic response to the Mid-Pleistocene Transition in the West Antarctic sector of the Southern Ocean. Marine Micropaleontology 92-93, 40-51.
Korff, L., von Dobeneck, T., Frederichs, T., Kasten, S., Kuhn, G., Gersonde, R., Diekmann, B., 2016. Cyclic magnetite dissolution in Pleistocene sediments of the abyssal northwest Pacific Ocean: Evidence for glacial oxygen depletion and carbon trapping. Paleoceanography 31, 600-624.

Krumhardt, K.M., Lovenduski, N.S., Debora Iglesias-Rodriguez, M., Kleypas, J.A., 2017. Coccolithophore growth and calcification in a changing ocean. Progress in Oceanography.
Kunz-Pirrung, M., Gersonde, R., Hodell, D.A., 2002. Mid-Brunhes century-scale diatom sea surface temperature and sea ice records from the Atlantic sector of the Southern Ocean (ODP Leg 177, sites 1093, 1094 and core PS2089-2). Palaeogeography, Palaeoclimatology, Palaeoecology 182, 305-328.
Lange, C., Berger, W., Lin, H.-L., Wefer, G., Leg, S.S.P., 1999. The early Matuyama diatom maximum off SW Africa, Benguela current system (ODP leg 175). Marine Geology 161, 93-114.
Lattaud, J., Lo, L., Zeeden, C., Liu, Y.-J., Song, S.-R., van der Meer, M.T., Damsté, J.S.S., Schouten, S., 2019. A multiproxy study of past environmental changes in the Sea of Okhotsk during the last 1.5 Ma. Organic Geochemistry 132, 50-61.
Lessard, E.J., Merico, A., Tyrrell, T., 2005. Nitrate : phosphate ratios and Emiliania huxleyi blooms. Limnology and Oceanography 50, 1020-1024.
Li, J., 2007. Carbon reservoir in low-latitude oceans and orbital cycles of monsoon climate (in Chinese with English abstract)(Ph. D. thesis). Tongji University, China.
Li, W., Wang, R., Xiang, F., Ding, X., Zhao, M., 2010. Sea surface temperature and subtropical front movement in the South Tasman Sea during the last 800 ka. Chinese Science Bulletin 55, 3338-3344.
Liang, D., Liu, C., 2018. Coccolith Assemblages and Primary Productivity Variations in the Central Western Pacific Warm Pool Over the Last 380 kyr. Journal of Ocean University of China 17, 563-570.
López-Otálvaro, G.-E., Flores, J.-A., Sierro, F.J., Cacho, I., 2008. Variations in coccolithophorid production in the Eastern Equatorial Pacific at ODP Site 1240 over the last seven glacial–interglacial cycles. Marine Micropaleontology 69, 52-69.
Lourens, L.J., 2004. Revised tuning of Ocean Drilling Program Site 964 and KC01B (Mediterranean) and implications for the δ18O, tephra, calcareous nannofossil, and geomagnetic reversal chronologies of the past 1.1 Myr. Paleoceanography 19.
Lupi, C., Bordiga, M., Sacchi, R., Ferretti, P., Cobianchi, M., 2019. Calcareous Nannofossil Response to Climate Variability During the Middle Pleistocene Transition in the Northwest Pacific Ocean (Ocean Drilling Program Leg 198 Site 1209). Paleoceanography and Paleoclimatology 34, 600-615.
Lyle, M., Baldauf, J., 2015. Biogenic sediment regimes in the Neogene equatorial Pacific, IODP Site U1338: Burial, production, and diatom community. Palaeogeography, Palaeoclimatology, Palaeoecology 433, 106-128.
Maiorano, P., Girone, A., Marino, M., Kucera, M., Pelosi, N., 2016. Sea surface water variability during the Mid-Brunhes inferred from calcareous plankton in the western Mediterranean (ODP Site 975). Palaeogeography, Palaeoclimatology, Palaeoecology.
Maiorano, P., Marino, M., Balestra, B., Flores, J.-A., Hodell, D., Rodrigues, T., 2015. Coccolithophore variability from the Shackleton Site (IODP Site U1385) through MIS 16-10. Global and Planetary Change 133, 35-48.
Marino, M., Maiorano, P., Tarantino, F., Voelker, A., Capotondi, L., Girone, A., Lirer, F., Flores, J.A., Naafs, B.D.A., 2014. Coccolithophores as proxy of seawater changes at orbital-to-millennial scale during middle Pleistocene Marine Isotope Stages 14–9 in North Atlantic core MD01-2446. Paleoceanography 29, 518-532.
McClelland, H.L., Bruggeman, J., Hermoso, M., Rickaby, R.E., 2017. The origin of carbon isotope vital effects in coccolith calcite. Nat Commun 8, 14511.
Misra, R., Bora, A., Dewangan, G., 2018. Estimation of error on the cross-correlation, phase and time lag between evenly sampled light curves. Astronomy and Computing 23, 83-91.
Murray, R., Knowlton, C., Leinen, M., Mix, A.C., Polsky, C., 2000. Export production and carbonate dissolution in the central equatorial Pacific Ocean over the past 1 Myr. Paleoceanography 15, 570-592.
Murray, R.W., Leinen, M., Knowlton, C.W., 2012. Links between iron input and opal deposition in

the Pleistocene equatorial Pacific Ocean. Nature Geoscience 5, 270-274.
Nissen, C., Vogt, M., Münnich, M., Gruber, N., Haumann, F.A., 2018. Factors controlling coccolithophore biogeography in the Southern Ocean. Biogeosciences 15, 6997-7024.
Paytan, A., Mclaughlin, K., 2007. The Oceanic Phosphorus Cycle. Chemical Reviews 107, 563-576.
Rickaby, R., Bard, E., Sonzogni, C., Rostek, F., Beaufort, L., Barker, S., Rees, G., Schrag, D., 2007. Coccolith chemistry reveals secular variations in the global ocean carbon cycle? Earth and Planetary Science Letters 253, 83-95.
Romero, O., Kim, J.H., Bárcena, M., Hall, I.R., Zahn, R., Schneider, R., 2015. High-latitude forcing of diatom productivity in the southern Agulhas Plateau during the past 350 kyr. Paleoceanography 30, 118-132.
Ruddiman, W.F., Kutzbach, J.E., 1989. Forcing of late Cenozoic northern hemisphere climate by plateau uplift in southern Asia and the American West. Journal of Geophysical Research: Atmospheres 94, 18409-18427.
Schmieder, F., von Dobeneck, T., Bleil, U., 2000. The Mid-Pleistocene climate transition as documented in the deep South Atlantic Ocean: initiation, interim state and terminal event. Earth and Planetary Science Letters 179, 539-549.
Sprenk, D., Weber, M.E., Kuhn, G., Rosén, P., Frank, M., Molina-Kescher, M., Liebetrau, V., Röhling, H.-G., 2013. Southern Ocean bioproductivity during the last glacial cycle–new detection method and decadal-scale insight from the Scotia Sea. Geological Society, London, Special Publications 381, 245-261.
Stoll, H.M., Rosenthal, Y., Falkowski, P., 2002a. Climate proxies from Sr/Ca of coccolith calcite: calibrations from continuous culture of Emiliania huxleyi. Geochimica et Cosmochimica Acta 66, 927-936.
Stoll, H.M., Ziveri, P., Geisen, M., Probert, I., Young, J.R., 2002b. Potential and limitations of Sr/Ca ratios in coccolith carbonate: new perspectives from cultures and monospecific samples from sediments. Philosophical Transactions of the Royal Society of London A: Mathematical, Physical and Engineering Sciences 360, 719-747.
Su, X., Liu, C., Beaufort, L., Tian, J., Huang, E., 2013. Late Quaternary coccolith records in the South China Sea and East Asian monsoon dynamics. Global and Planetary Change 111, 88-96.
Sun, H., Li, T., Chang, F., Wan, S., Xiong, Z., An, B., Sun, R., 2017. Deep-sea carbonate preservation in the western Philippine Sea over the past 1Ma. Quaternary International 459, 101-115.
Sun, H., Li, T., Sun, R., Yu, X., Chang, F., Tang, Z., 2011. Calcareous nannofossil bioevents and microtektite stratigraphy in the Western Philippine Sea during the Quaternary. Chinese Science Bulletin 56, 2732-2738.
Suzuki, T., 2013. PACIFICA Data Synthesis Project. ORNL/CDIAC-159, NDP-092. Carbon Dioxide Information Analysis Center.
Sviben, S., Gal, A., Hood, M.A., Bertinetti, L., Politi, Y., Bennet, M., Krishnamoorthy, P., Schertel, A., Wirth, R., Sorrentino, A., Pereiro, E., Faivre, D., Scheffel, A., 2016. A vacuole-like compartment concentrates a disordered calcium phase in a key coccolithophorid alga. Nat Commun 7, 11228.
Tian, J., Wang, P., Cheng, X., Li, Q., 2002. Astronomically tuned Plio–Pleistocene benthic δ< sup> 18</sup> O record from South China Sea and Atlantic–Pacific comparison. Earth and Planetary Science Letters 203, 1015-1029.
Tyrrell, T., 1999. The relative influences of nitrogen and phosphorus on oceanic primary production. Nature 400, 525-531.
Wang, R., Jian, Z., Xiao, W., Tian, J., Li, J., Chen, R., Zheng, Y., Chen, J., 2007. Quaternary biogenic opal records in the South China Sea: Linkages to East Asian monsoon, global ice volume and orbital forcing. Science in China Series D: Earth Sciences 50, 710-724.
Xuan, C., Channell, J.E.T., Hodell, D.A., 2016. Quaternary magnetic and oxygen isotope stratigraphy in diatom-rich sediments of the southern Gardar Drift (IODP Site U1304, North Atlantic). Quaternary Science Reviews 142, 74-89.
Zhang, H., Liu, C., Jin, X., Shi, J., Zhao, S., Jian, Z., 2016. Dynamics of primary productivity in the

northern South China Sea over the past 24,000 years. Geochemistry, Geophysics, Geosystems.
Zhou, C., Jin, H., Jian, Z., 2011. Variations of the late quaternary paleo-productivity in the western equatorial Pacific: evidences from the elemental ratios. Quaternary Sciences 31, 276-283.